Application of Incremental Dynamic Analysis to an RC- Structure

Article · January 2003

3 authors, including:

F. Jalayer
University of Naples Federico II
75 PUBLICATIONS   **1,387** CITATIONS

Some of the authors of this publication are also working on these related projects:

CLUVA, CLimate change and Urban Vulnerability in Africa View project

APPLICATION OF INCREMENTAL DYNAMIC ANALYSIS TO AN RC-STRUCTURE

Dimitrios VAMVATSIKOS[1]   Fatemeh JALAYER[2]   C. Allin CORNELL[3]

[1] divamva@stanfordalumni.org, Theagenous 11, Athens 11634, GREECE
[2] fjalayer@stanford.edu, Dept. of Civil and Environmental Engng, Stanford University, Stanford, USA
[3] cornell@stanford.edu, Dept. of Civil and Environmental Engng, Stanford University, Stanford, USA

1 INTRODUCTION

Of great interest in Performance-Based Earthquake Engineering (PBEE) is the accurate estimation of the seismic performance of structures, and in particular, the mean annual frequency (MAF) of exceeding a specified structural demand or a certain limit-state capacity (e.g., Immediate Occupancy or Collapse Prevention, FEMA [1, 2]). To accomplish the task several important methods have emerged, a promising one being Incremental Dynamic Analysis (IDA), Vamvatsikos and Cornell [3], a computer-intensive procedure that offers thorough (demand and capacity) prediction capability by using a series of nonlinear dynamic analyses under suitably multiply-scaled ground motion records. While it is a simple concept, performing an IDA requires several important steps:

1   Create an appropriate model for the structure under investigation.
2   Select a suite of ground motion records.
3   For each record, incrementally scale it to multiple levels and run a nonlinear dynamic analysis each time. Stop incrementing when numerical non-convergence is first encountered.
4   Select a ground motion Intensity Measure *IM* (e.g., $S_a(T_1, 5\%)$, the 5%-damped first-mode spectral acceleration) and a Damage Measure *DM* (e.g., $\theta_{\max}$, the maximum over all stories peak interstory drift ratio) and postprocess the results of the dynamic analyses:
    i   Interpolate the resulting *IM*, *DM* points to generate an IDA curve for each individual record.
    ii   Define limit-states and estimate the corresponding capacities on each IDA curve.
    iii Summarize the IDA curves and limit-state capacities across all records into 16%, 50% and 84% fractiles.
    iv   Integrate with the results of Probabilistic Seismic Hazard Analysis and calculate MAFs of exceeding each limit-state.
5   Use the IDA data to better understand the behavior of the structure.

In the following sections we are going to provide a practical example of the methodology by applying IDA on a medium-height older reinforced-concrete structure. We are going to guide the reader through all of the above steps, explain the reasoning behind our choices and make some important general observations about the structural behavior under seismic loads.

2 MODEL AND GROUND MOTION RECORD SELECTION

We have selected the Holiday Inn Hotel in Van Nuys, CA, as a comprehensive case study in probabilistic assessment of an older reinforced concrete structure (Jalayer [4]). This structure is serving as a test-bed for the activities of the Pacific Earthquake Engineering Research Center (PEER [5]). It is a a 7-story hotel located in California's San Fernando Valley, northwest of downtown Los Angeles. The hotel was designed in 1965 according to the 1964 Los Angeles City Building Code, and built in 1966. In plan, the building is rectangular, 19.2m by 45.7m, 3 bays by 8 bays, 7 stories tall. The structural system is a reinforced concrete moment-frame with flat-plate slabs, but the reinforcing steel lacks ductile detailing.

We chose one of the transverse frames (Figure 1) to form a centerline model that has a first-mode period of T_1 = 0.8 sec. We were interested in modeling the challenging issues of cyclic stiffness and strength degradation behavior in reinforced concrete. Hence, the members are modeled using a beam-column element developed by Pincheira *et al.* [6] that incorporates stiffness and strength-degrading hysteretic behavior in both shear and flexure. The degrading behavior is concentrated in two rotational springs at the two ends (flexure) and a translation spring somewhere in the middle of the element

Table 1 The suite of twenty ground motion records used.

No	Event	Station	ϕ° [1]	Soil[2]	M[3]	R[4] (km)	PGA (g)
1	Northridge, 1994	LA, Baldwin Hills	090	B,B	6.7	31.3	0.239
2	Imperial Valley, 1979	Compuertas	285	C,D	6.5	32.6	0.147
3	Imperial Valley, 1979	Plaster City	135	C,D	6.5	31.7	0.057
4	Loma Prieta, 1989	Hollister Diff. Array	255	–,D	6.9	25.8	0.279
5	San Fernando, 1971	LA, Hollywood Stor. Lot	180	C,D	6.6	21.2	0.174
6	Loma Prieta, 1989	Coyote Lake Dam Downstream	285	B,D	6.9	22.3	0.179
7	Imperial Valley, 1979	Cucapah	085	C,D	6.5	23.6	0.309
8	Northridge, 1994	LA, Hollywood Storage FF	360	C,D	6.7	25.5	0.358
9	Loma Prieta, 1989	Anderson Dam Downstream	360	B,D	6.9	21.4	0.24
10	Loma Prieta, 1989	Hollister South & Pine	000	–,D	6.9	28.8	0.371
11	Loma Prieta, 1989	Sunnyvale Colton Ave	360	C,D	6.9	28.8	0.209
12	Superstition Hills, 1987	Wildlife Liquefaction Array	090	C,D	6.7	24.4	0.18
13	Imperial Valley, 1979	Chihuahua	282	C,D	6.5	28.7	0.254
14	Imperial Valley, 1979	El Centro Array #13	230	C,D	6.5	21.9	0.139
15	Imperial Valley, 1979	Westmoreland Fire Station	180	C,D	6.5	15.1	0.11
16	Loma Prieta, 1989	Halls Valley	090	C,C	6.9	31.6	0.103
17	Superstition Hills, 1987	Wildlife Liquefaction Array	360	C,D	6.7	24.4	0.2
18	Imperial Valley, 1979	Compuertas	015	C,D	6.5	32.6	0.186
19	Imperial Valley, 1979	Plaster City	045	C,D	6.5	31.7	0.042
20	San Fernando, 1971	LA, Hollywood Stor. Lot	090	C,D	6.6	21.2	0.21

[1] Component   [2] USGS, Geomatrix soil class   [3] moment magnitude   [4] closest distance to fault rupture
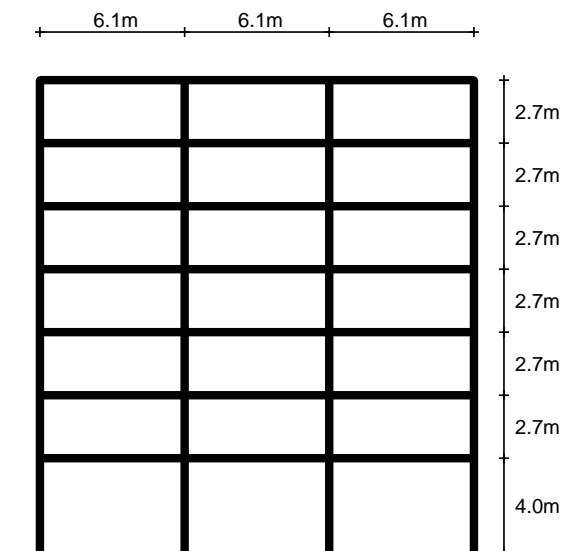

Fig. 1 The structural model used for the Van Nuys Holiday Inn frame.

(shear). All analyses were performed with DRAIN2D-UW (Dotiwala *et al.* [7]) that is a modified version of DRAIN-2D (Powell [8]) produced in the University of Wisconsin.

In addition we need a suite of ground motion records. Previous studies (Shome and Cornell [9]) have shown that for mid-rise buildings, ten to twenty records are usually enough to provide sufficient accuracy in the estimation of seismic demands, assuming a relatively efficient *IM*, like $S_a(T_1, 5\%)$, is used. Consequently, we have selected a set of twenty ground motion records, listed in Table 1, that belong to a bin of relatively large magnitudes of 6.5 – 6.9 and moderate distances, all recorded on firm soil and bearing no marks of directivity. The selected ground motions are effectively presumed to be representative of events likely to cause severe ground motions at the Van Nuys site.

3 PERFORMING THE ANALYSIS

Once the model has been formed and the ground motion records have been selected, we need a fast and automated way to perform the actual nonlinear dynamic analyses required for IDA. This entails

appropriately scaling each record to cover the entire range of structural response, from elasticity, to yielding, and finally global dynamic instability.

We chose to use a *stepping* algorithm to trace the IDA curves of this building (Vamvatsikos and Cornell [3]). Although there do exist better algorithms to choose the *IM*-levels, like the *hunt & fill* (Vamvatsikos and Cornell [10]), the stepping algorithm is by far the easiest to understand and program. Analyses are performed at increasing levels of *IM* at constant steps, until numerical non-convergence is encountered (signaling global dynamic instability). The user only needs to specify the desired *IM*-step size, select the maximum tolerable number of dynamic analyses, and then wait for a few hours to get the results. Since the algorithm has been implemented in software (Vamvatsikos and Cornell [11]) that is able to wrap around most existing analysis programs (e.g., DRAIN-2D, Powell [8]), it renders IDA almost effortless, needing no human supervision.

As an example, we will show in detail the sequence of runs performed by the stepping algorithm when tracing record #11 from Table 1. To express the scaling level we need an initial, temporary choice of *IM*, and we have chosen $S_a(T_1, 5\%)$, a decision that need not restrict us in any way: scaling can be re-expressed in terms of any other *scalable IM* (Vamvatsikos and Cornell [3]) that we wish after the runs have been performed. Hence, in $S_a(T_1, 5\%)$ terms, the algorithm was configured to use an initial step of 0.1g while a maximum of 20 runs was allowed for each record. Thus, we have selected by default a resolution of 0.1g on the global collapse capacity, i.e., we expect the model to develop numerical non-convergence and show practically infinite θ_{max} at some high intensity level, and we wish this level to be known within 0.1g of its *IM*-value.

As seen in Table 2, the algorithm constantly increased the *IM* in steps of 0.1g from 0 up to 0.7g. That is where global instability was encountered for the first time thus terminating the IDA tracing for this record. In total, only 7 runs were expended.

Table 2 Sequence of runs generated by the stepping algorithm for record #11.

No.	1	2	3	4	5	6	7
$S_a(T_1, 5\%)$	0.1	0.2	0.3	0.4	0.5	0.6	0.7
θ_{max}	0.21%	0.53%	0.83%	1.63%	3.45%	7.26%	$+\infty$

4 POSTPROCESSING

Equally important to the analysis is the postprocessing of the resulting data and perhaps the most important issue is selecting a suitable *IM* and *DM*. There are several issues of efficiency and sufficiency associated with the *IM* selection (Luco and Cornell [12]). Since there are no directivity-influenced records in our suite and the building is of medium height (hence first-mode-dominated), the 5%-damped first-mode spectral acceleration $S_a(T_1, 5\%)$ will be our choice; it has been proven to be both efficient, by minimizing the scatter in the results, requiring only a few ground motion records to provide good demand and capacity estimates, and sufficient, as it provides a complete characterization of the response without the need for magnitude or source-to-site distance information (Shome and Cornell [9]). Similarly, selecting a *DM* can be application-specific; for example, the peak floor accelerations are correlated with contents' damage and many types of non-structural elements' damage, while the maximum peak interstory drift ratio θ_{max} (the maximum over time and over all stories of the interstory drift ratios recorded during the timehistory analysis) is known to relate well (FEMA [1]) to global dynamic instability and several structural performance limit-states upon which we intend to focus. Therefore, θ_{max} will be our *DM*-choice. Still, it must be emphasized that these *IM* and *DM* choices are by no means limiting. Assuming that additional *DM*s have been recorded from the analyses, they can be substituted instead of θ_{max}, and by employing the postprocessing techniques presented, the IDA data can also be expressed in a different scalable *IM*, without any need to rerun the dynamic analyses.

Having selected our *IM* and *DM*, we are still faced with an abundance of IDA-generated data that need to be sorted out and presented in meaningful ways. It is a time-consuming and challenging task that we are going to step our way through, but it can be rendered totally effortless with the proper software. Actually, most of what follows is a direct description of the inner workings of an automated postprocessing program (Vamvatsikos and Cornell [11]), whose graphical output appears in the accompanying figures.

4.1 Generating the IDA curves by interpolation

Once the desired *IM* and *DM* values (in our case $S_a(T_1, 5\%)$ and θ_{max}) are extracted from each of the dynamic analyses, we are left with a set of discrete points for each record that reside in the *IM-DM* plane
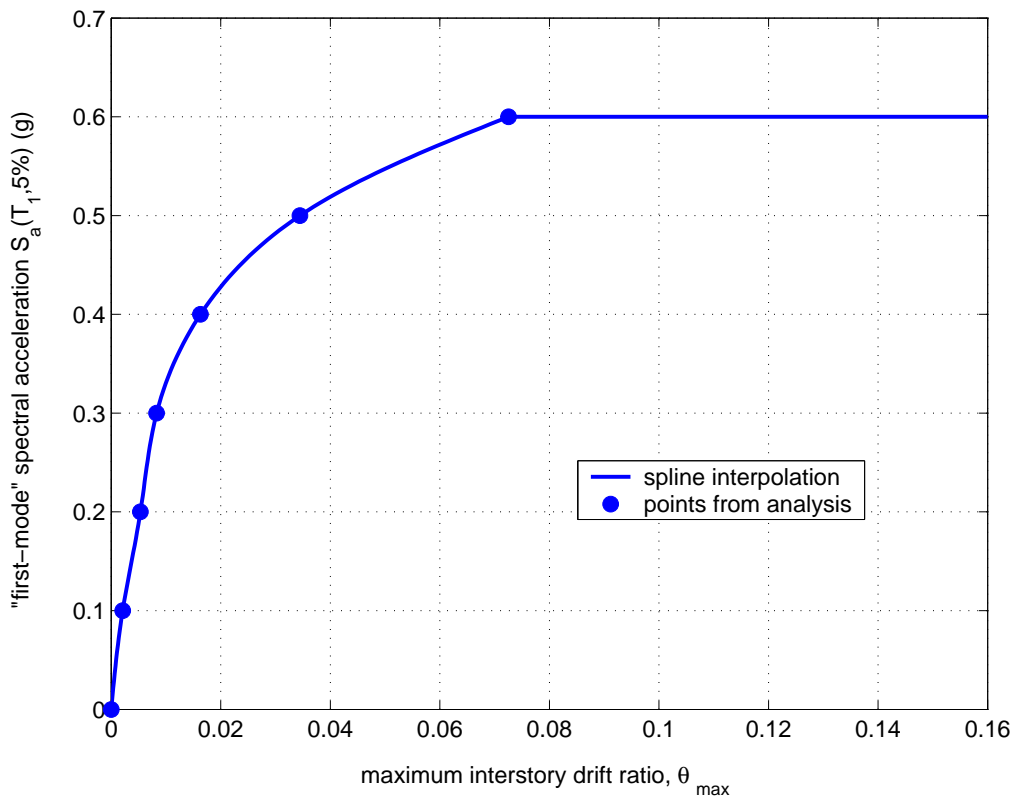
Fig. 2 The numerically-converging dynamic analysis points for record #11 are interpolated using a spline approximation.
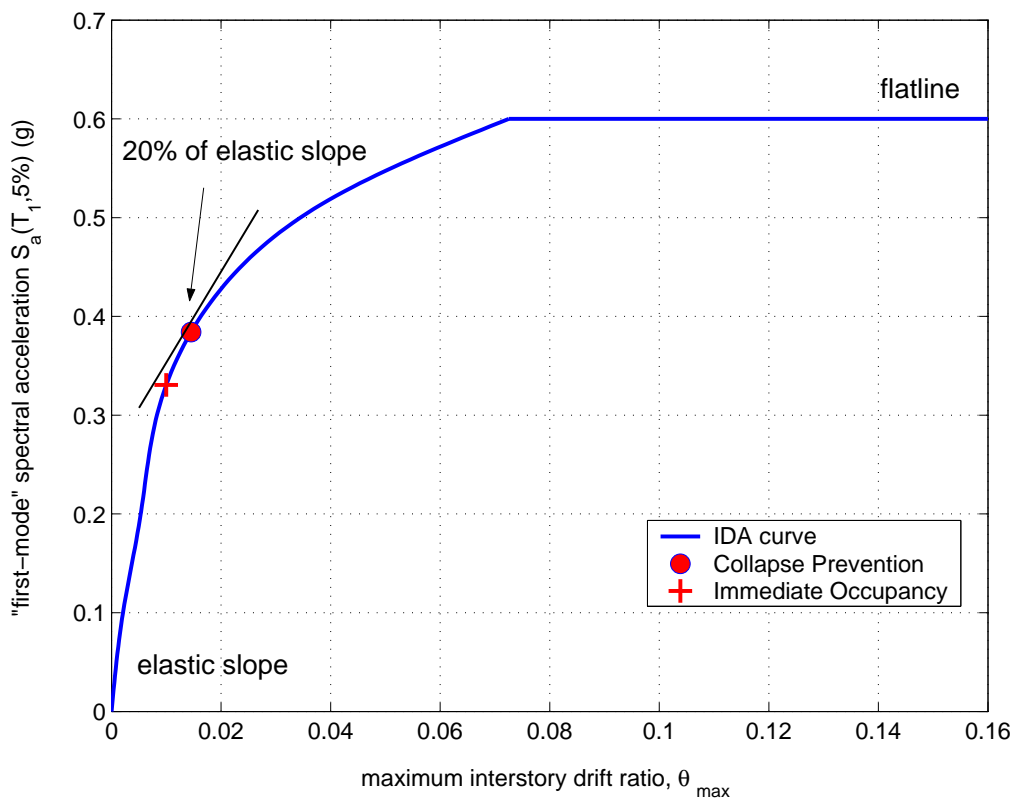

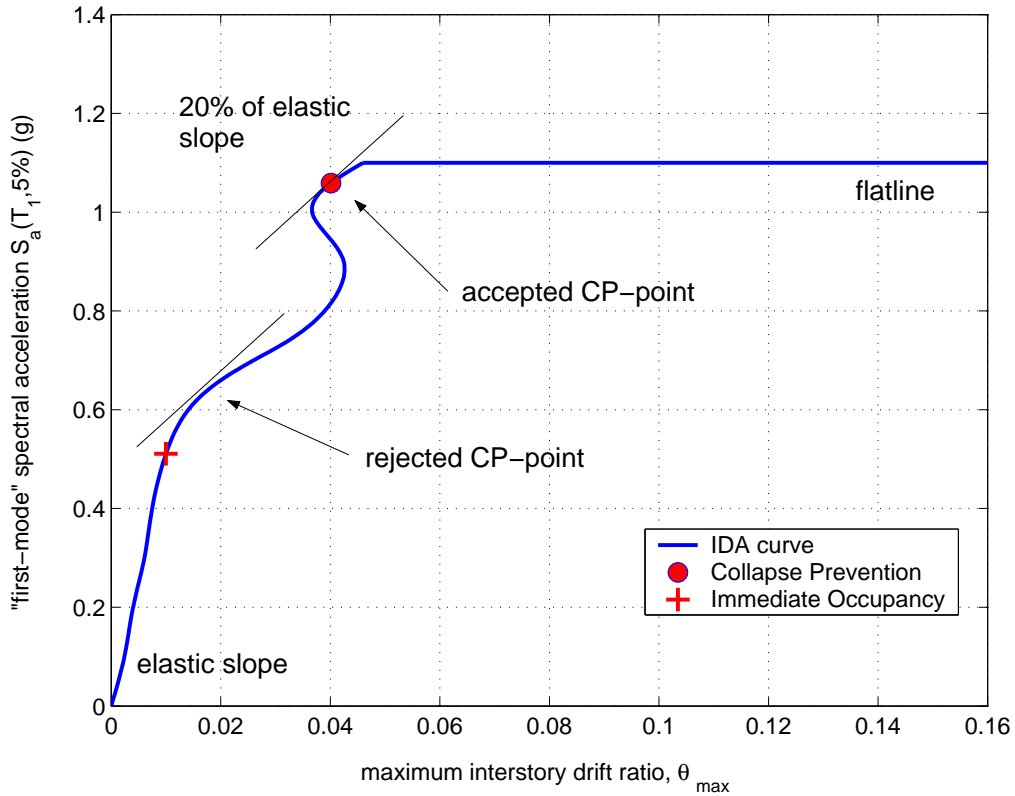**Fig. 3** The limit-states, as defined on the IDA curve of record #11.

Fig. 4 The limit-states, as defined on the IDA curve of record #3. Note the extreme hardening that causes the appearance of multiple possible CP points, the highest of which (in *IM*-terms) is the accepted one.
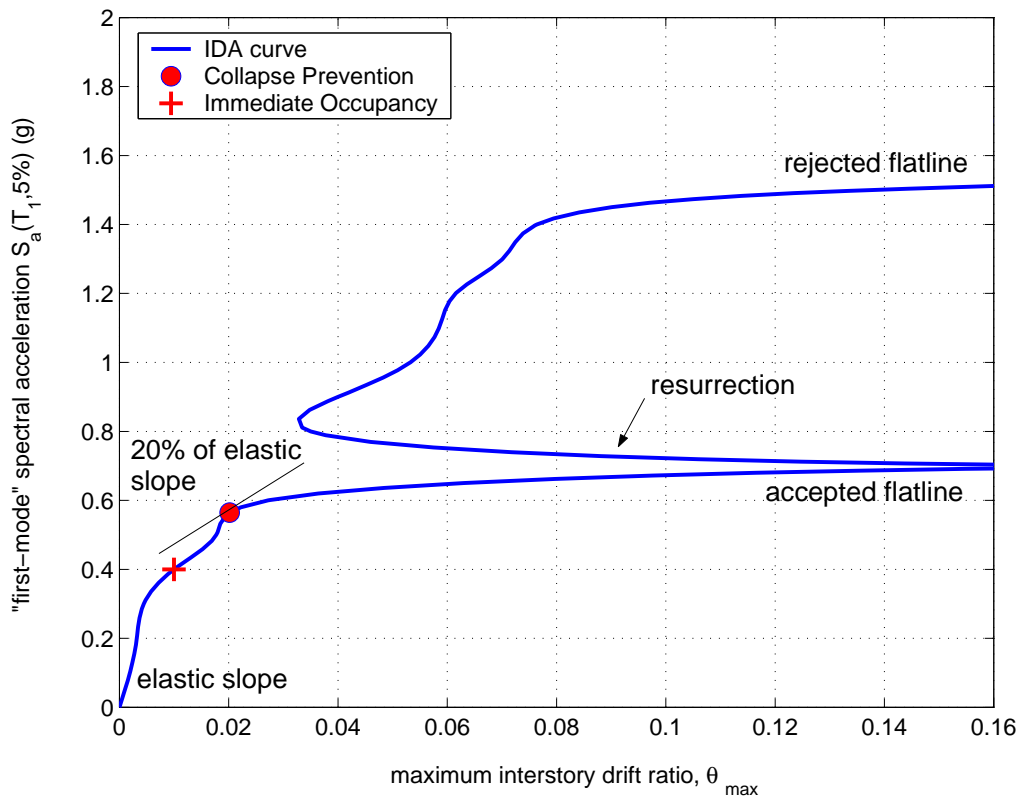

Fig. 5 The limit-states, as defined on the IDA curve of record #19. Resurrection causes the appearance of a higher flatline (in *IM*-terms) that is rejected.

Table 3 The *IM* and *DM* values of capacity for all records and each limit-state.

No	$S_a(T_1,5\%)$ (g)			θ_{max}		
	IO	CP	GI	IO	CP	GI
1	0.66	1.03	1.10	0.100	0.025	$+\infty$
2	0.46	0.90	1.23	0.100	0.034	$+\infty$
3	0.51	1.06	1.10	0.100	0.040	$+\infty$
4	0.75	1.51	1.69	0.100	0.027	$+\infty$
5	0.42	0.64	0.90	0.100	0.016	$+\infty$
6	0.55	1.81	1.97	0.100	0.073	$+\infty$
7	0.41	0.78	0.97	0.100	0.031	$+\infty$
8	0.59	1.33	1.71	0.100	0.023	$+\infty$
9	0.65	0.85	1.00	0.100	0.019	$+\infty$
10	0.38	1.57	1.66	0.100	0.046	$+\infty$
11	0.33	0.38	0.60	0.100	0.015	$+\infty$
12	0.33	0.50	0.70	0.100	0.022	$+\infty$
13	0.68	1.58	1.70	0.100	0.033	$+\infty$
14	0.44	0.72	0.90	0.100	0.029	$+\infty$
15	0.53	0.68	1.00	0.100	0.020	$+\infty$
16	0.49	1.08	1.18	0.100	0.026	$+\infty$
17	0.44	1.02	1.10	0.100	0.053	$+\infty$
18	0.58	0.97	1.05	0.100	0.022	$+\infty$
19	0.40	0.56	0.69	0.100	0.020	$+\infty$
20	0.46	0.90	0.90	0.100	0.041	$+\infty$

and lie on its IDA curve, as in Figure 2. By interpolating them, the entire IDA curve can be approximated without performing additional analyses. To do so, we may use a basic piecewise linear approximation, or the superior spline interpolation. Based on the concept of natural, coordinate-transformed, parametric splines with a centripetal scheme for knot-selection (Farin [13], Lee [14]), a realistic interpolation can be generated that accurately represents the real IDA curve, as shown in Figure 2 for our example of record #11 (Table 2). Having the complete curve available, it is now possible to calculate *DM* values at arbitrary levels of *IM*, allowing the extraction of more (*IM*, *DM*) points with a minimum of computation.

The smooth IDA curve provided by the interpolation scheme offers much to observe. For record #11, depicted in Figure 2, the IDA curve is quite simple. It starts as a straight line in the elastic range and then shows the effect of early yielding and local damage by having some slight changes in the local tangent slope but in general it stays on the elastic slope, following the well-known "equal-displacement" rule for moderate-period structures (Veletsos and Newmark [15]); thus, at any given $S_a(T_1,5\%)$-level below 0.3g it maintains about the same displacement as an elastic system. Then, at $S_a(T_1,5\%) \approx 0.3$g it starts *softening*, showing ever decreasing tangent slopes, i.e., greater rates of *DM* accumulation as *IM* increases, reaching the "flatline" slightly above $S_a(T_1,5\%) = 0.6$g, where the structure responds with practically "infinite" θ_{max} values and numerical non-convergence has been encountered during the analysis. That is when the building has reached global dynamic instability, when a small increment in the *IM*-level results in unlimited increase of the *DM*-response.

IDA curves are not always this simple. As we are going to see in later sections, the small wiggles that appear (Figure 2) between the end-of-elasticity and the flatline can become much larger and practically dominate the shape of the curve.

4.2 Defining limit-states on an IDA curve

In order to be able to do the performance calculations needed for PBEE, we need to define limit-states on the IDA curves. For our case study, we chose to demonstrate three: Immediate Occupancy (IO), Collapse Prevention (CP), both defined in FEMA [1, 2], and global dynamic instability (GI). For this older reinforced-concrete frame that we are studying we have decided to set the IO limit-state to appear at θ_{max} = 1%. We have chosen to follow the FEMA [1] guidelines to define the CP point, which is thus not exceeded on the IDA curve until the final point where the local tangent reaches 20% of the elastic slope (Figure 3) or θ_{max} = 10%, whichever occurs first in *IM* terms. The main idea is to place the CP

limit-state at a point where the IDA curve is softening towards the flatline but at low enough values of θ_{max} (less than 10%) so that we still trust the structural model. Finally, GI happens when the flatline is reached and any increase in the *IM* results in practically infinite *DM* response.

It is easy to calculate the *IM*-values for the IO limit-state; all we need to do is to calculate all the *IM*-values that produce θ_{max} = 1% and, if more than one, select the lowest. This is the one that signals the very first exceedance of the IO limit-state for the given record. For our example of record #11 in Figure 3, IO is violated for $S_a(T_1, 5\%) \geq 0.33g$ or $\theta_{max} \geq 1\%$.

According to the CP limit-state concept, we need to find the highest (in *IM*-value) point where the IDA tangent slope is equal to 20% of the elastic. This point usually lies on the softening segment that precedes the flatline. Additionally, another candidate point is at θ_{max} = 10%; therefore whichever comes first (in *IM*), the slope or the θ_{max} limit, decides the CP capacity. The simple IDA curve shape of record #11 (Figure 3) makes this calculation relatively easy. The 20%-slope rule governs and generates only one candidate point; thus, CP is violated for $S_a(T_1, 5\%) \geq 0.38g$ or $\theta_{max} \geq 1.5\%$.

On the other hand, record #3 (Figure 4) has a much more complicated shape. The IDA starts *softening* at about 0.6g by displaying a tangent slope less than the elastic but subsequently it *hardens* having a local slope higher that the elastic. Actually the *DM*-response of the building is higher at $S_a(T_1, 5\%) = 0.9g$ than it is at $S_a(T_1, 5\%) = 1g$. The IDA starts to *soften* again only after $S_a(T_1, 5\%) \approx 1.05g$ as it blends into the flatline. This phenomenon of *hardening* generates two possible locations where the local slope is 20% of the elastic, as shown in Figure 4. Obviously, the lower one (in *IM*-terms) should be rejected, as it does not directly precede a flatline. This indicates that the building is not close to global collapse yet as the CP limit-state definition requires. Thus, CP is exceeded for record #3 only when $S_a(T_1, 5\%) \geq 1.06g$, thus 1.06g is the *IM*-value of the CP limit-state capacity. While the corresponding *DM*-value of capacity is θ_{max} = 4% (as defined by FEMA [1]), it is not correct to state that the CP limit-state is violated for $\theta_{max} \geq 4\%$ for this record. The segment of the IDA between 0.81g and 0.95g also satisfies the inequality $\theta_{max} \geq 4\%$, but it lies at lower $S_a(T_1, 5\%)$-values which do not violate the CP limit-state. Such problems appear often when defining limit-states on IDAs with serious hardening.

Calculating the *IM*-value of the flatline capacity is usually simple, as our best estimate is actually somewhere between the highest numerically-converging run and the lowest non-converging one, as produced by the stepping algorithm. We choose to use the *IM*-value of the highest numerically-converging run as the estimate, e.g., $S_a(T_1, 5\%) = 0.6g$ for record #11, Table 2. We could have used, for example, the average of the highest converging and lowest non-converging run, $(0.6 + 0.7)/2 = 0.65g$, but the difference is negligible and gets smaller and smaller as we decrease the step-size in the stepping algorithm.

Again, the shapes of IDA curves can sometimes make this calculation a challenge. The hardening phenomenon observed in Figure 4 can be so extreme for some records as to bring the structure back from global collapse. This is the phenomenon of *structural resurrection* that appears for record #19 in Figure 5. Although the structure has encountered global instability at $S_a(T_1, 5\%) = 0.69g$, it is *resurrected* at higher $S_a(T_1, 5\%)$-levels and re-enters global instability only at $S_a(T_1, 5\%) = 1.52g$. Which of the two flatlines should we select? Obviously we are interested in the earliest failure of the structure, thus GI occurs at the lowest (in *IM*-terms) flatline, at $S_a(T_1, 5\%) = 0.69g$.

In this systematic manner we can estimate the IO, CP and GI limit-state capacities for all records, as seen in Table 3, and then proceed to the next stage in our development.

4.3 Summarizing the IDAs

By generating the IDA curve for each record and subsequently defining the limit-state capacities, a large amount of data can be gathered, only part of which is seen in Figure 6. There, the IDA curves display a wide range of behavior, showing large record-to-record variability, thus making it essential to summarize such data and quantify the randomness introduced by the records. We need to employ appropriate summarization techniques that will reduce this data to the distribution of *DM* given *IM* and to the probability of exceeding any specific limit-state given the *IM* level.

The limit-state capacities can be easily summarized into some central value (e.g., the mean or the median) and a measure of dispersion (e.g., the standard deviation, or the difference between two fractiles). Consequently, we have chosen to calculate the 16%, 50% and 84% fractile values of *DM* and *IM* capacity for each limit-state, as shown in Table 4, and also graphically depicted in Figure 7. For example, reading off Table 4, at $S_a(T_1, 5\%) = 0.94g$ or equivalently at $\theta_{max} = 0.026$, 50% of the ground motion records have forced the 7-story structure to violate CP.

There are several methods to summarize the IDA curves, but the cross-sectional fractiles are arguably the most flexible and robust with respect to the infinite *DM*s introduced by the flatlines (Vamvatsikos and
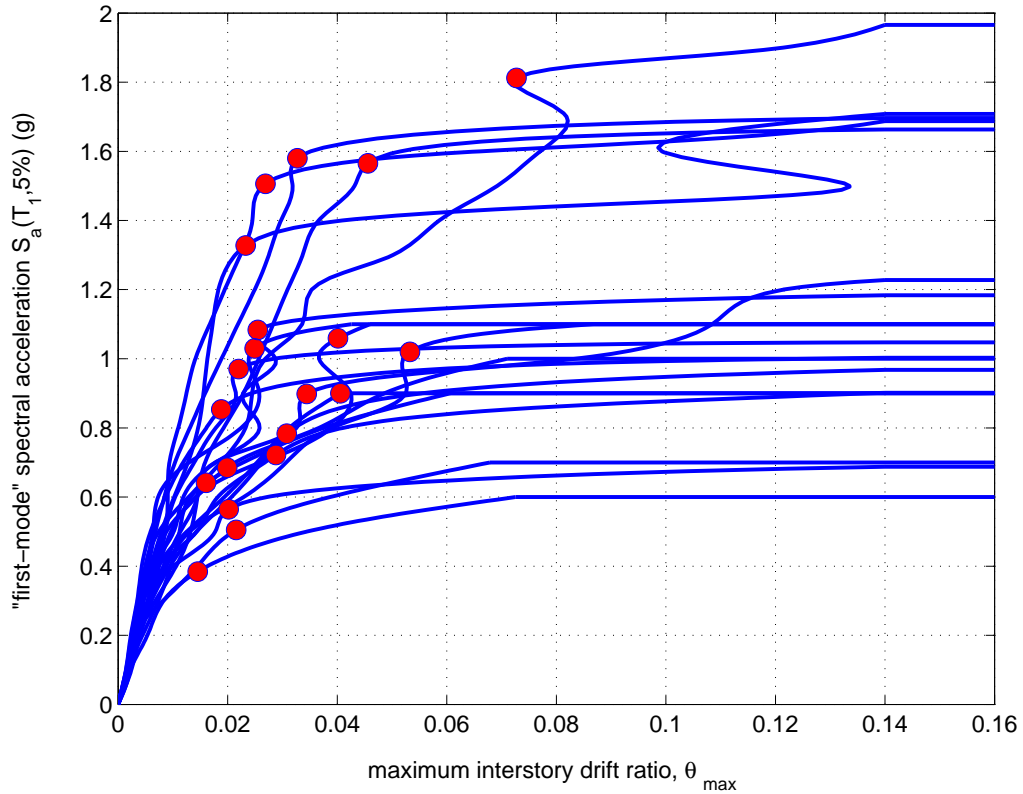
Fig. 6 All twenty IDA curves and the associated limit-state capacities. The IO limit is at the intersection of each IDA with the θ_{max} = 1% line, the CP limit is represented by the dots, while GI occurs at the flatlines.
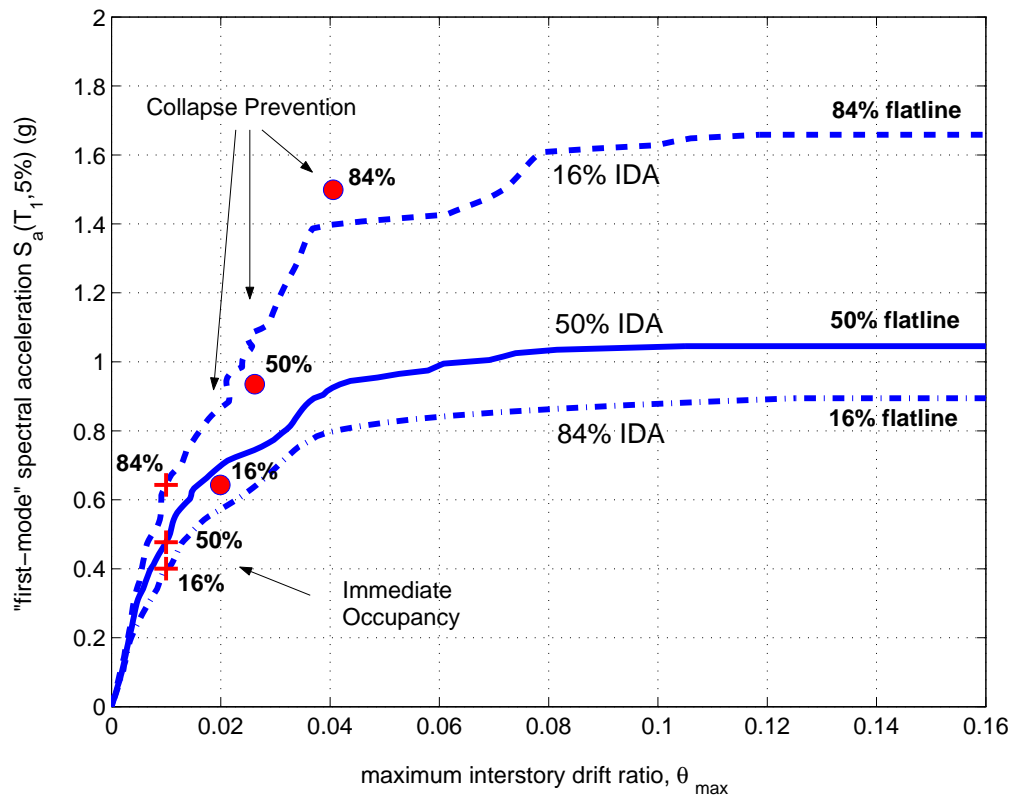

Fig. 7 The summary of the IDA curves and corresponding limit-state capacities into their 16%, 50% and 84% fractiles.

Table 4 Summarized capacities for each limit-state.

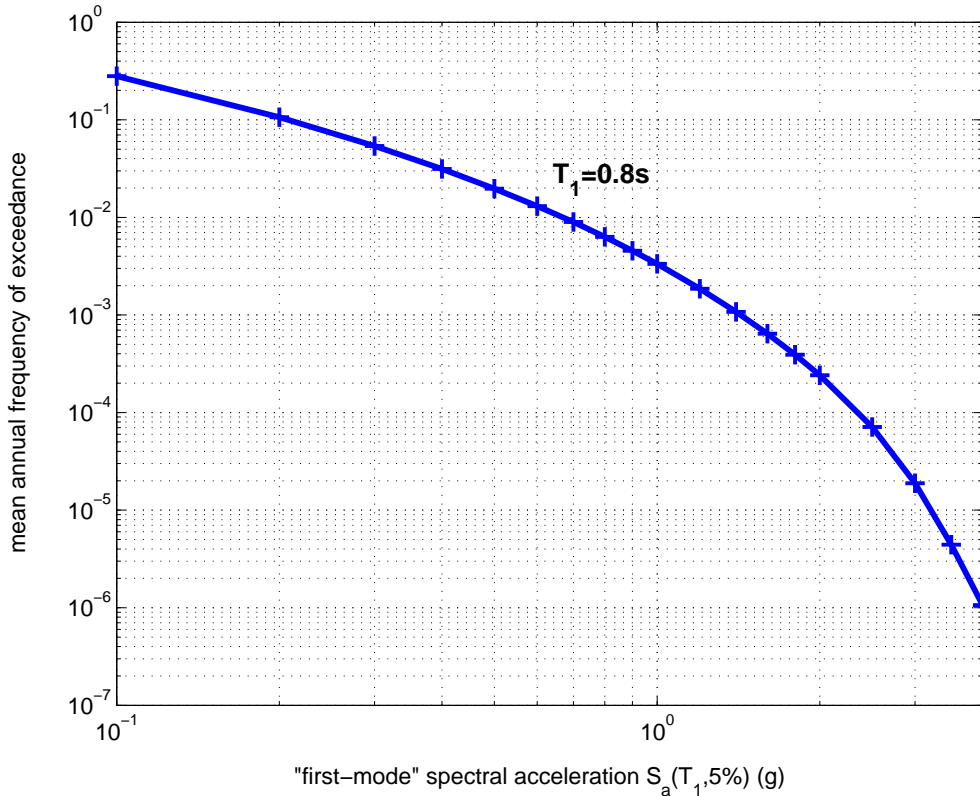|	$S_a(T_1, 5\%)$ (g)			θ_{max}		
	IO	CP	GI	IO	CP	GI
16%	0.40	0.64	0.90	0.010	0.020	$+\infty$
50%	0.48	0.94	1.07	0.010	0.026	$+\infty$
84%	0.64	1.50	1.69	0.010	0.041	$+\infty$

Fig. 8 Hazard curve λ_{IM} for the Van Nuys Los Angeles site, for $S_a(0.8s, 5\%)$ as the *IM*.

Cornell [3]). Using the spline interpolation we can generate stripes of *DM*-values at arbitrary levels of the *IM*; each stripe contains twenty *DM*-values, one for each record, that may be finite or even infinite when a record has already reached its flatline at a lower *IM*-level. By summarizing the *DM*-values for each stripe into their 16%, 50% and 84% percentiles, we get fractile values of *DM* given *IM* that are in turn interpolated for each fractile to generate the 16%, 50% and 84% fractile IDA curves, shown in Figure 7. For example, given $S_a(T_1, 5\%)$ = 0.8g, 16% of the records produce $\theta_{max} \leq 1.6\%$, 50% of the records $\theta_{max} \leq 3.2\%$ and 84% $\theta_{max} \leq 4\%$. Under suitable assumptions of continuity and monotonicity of the IDA curves (Vamvatsikos and Cornell [10]), the fractiles can also be used in the inverse way, e.g., in order to generate demand $\theta_{max} = 4\%$, 84% of the records need to be scaled at levels $S_a(T_1, 5\%) \geq 0.8g$, 50% of the records at $S_a(T_1, 5\%) \geq 0.93g$ and 16% at $S_a(T_1, 5\%) \geq 1.4g$. Consequently, the 16%, 50% and 84% IO points and GI flatlines actually reside on the 84%, 50% and 16% IDA curves respectively, a direct result of the definition of these limit-states. On the other hand, no such general property exists for the CP points, but experience has shown that they usually lie quite close and often on top of their corresponding fractile IDAs, just like the other fractile limit-state points.

4.4 PBEE calculations

One of the goals of PBEE is producing MAFs of exceedance for the limit-states. This can be easily accomplished with the summarized results that have been calculated so far, especially if one considers the formats proposed by SAC/FEMA (FEMA [1, 2]) or by the Pacific Earthquake Engineering Research Center (Cornell and Krawinkler [16]). The process invariably involves calculating the MAF of exceeding values of the chosen *IM*, readily available for $S_a(T_1, 5\%)$ from conventional PSHA, and appropriately
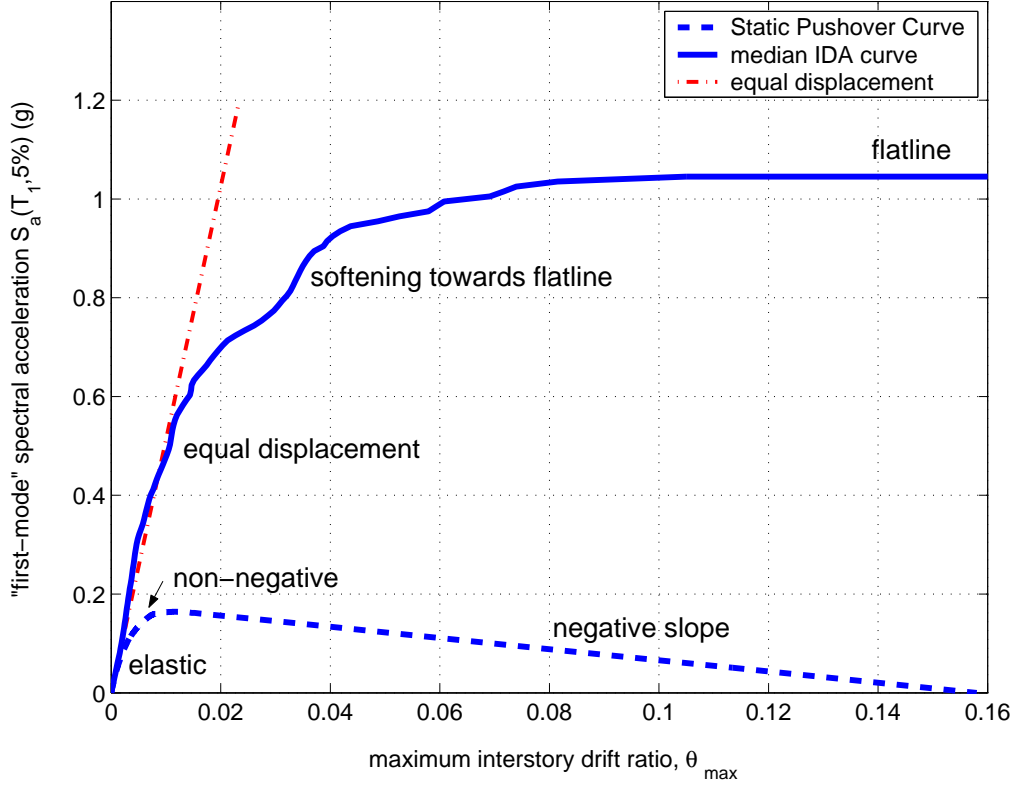
Fig. 9 The SPO curve generated from a first-mode load pattern versus the median IDA.

integrating with the conditional probabilities of exceeding each limit-state (given the *IM* or *DM* level) to produce the desired MAFs of limit-state exceedance. It is a relatively straightforward method that has been described in extent, for example, by Cornell *et al.* [17].

Here we will perform such calculations using a form of the framing equation adopted by the Pacific Earthquake Engineering Research Center (Vamvatsikos and Cornell [3, 10], Cornell and Krawinkler [16]),

$$\lambda_{\text{LS}} = \int_{x=0}^{x=+\infty} F_{IM^c}(x) \left| \frac{d\lambda_{IM}(x)}{dx} \right| dx \tag{1}$$

where λ_{LS} is the MAF of exceeding the given limit-state. The quantity in the absolute value is the *IM* hazard gradient, i.e., the first derivative of the hazard curve λ_{IM} with respect to the *IM*. Finally, $F_{IM^c}(x)$ is the Cumulative Distribution Function (CDF) of the *IM*-value of limit-state capacity. In this case, all quantities in Eq. (1) are known, and only a single numerical integration over the values of *IM* (or *x*) is needed to calculate λ_{LS} and get the values of Table 5. Additionally, by inverting λ_{LS} we can get the (mean) return period of limit-state exceedance. So, reading off Table 5, we have that the IO limit-state is on average exceeded once every 36 years, the CP limit-state once every 91 years and the GI limit-state only once every 185 years. Still, we should view these numbers with caution as the MAFs and return periods are bound to change if we properly take into account the epistemic uncertainty associated with our imperfect knowledge, e.g., of the structural properties (Cornell *et al.* [17]).

Table 5 MAFs of exceedance and corresponding return periods for violating each limit-state, calculated numerically from Eq. (1) and the hazard curve of Figure 8.

	IO	CP	GI
MAF of exceedance	0.0278	0.0109	0.0054
return period (years)	36	91	185

4.5 SPO versus IDA

Beyond the essential calculations needed for PBEE, there is much more information that we could easily glean out of the IDA by taking a closer look at the results and plotting them in new ways. In

particular, it is very informative to visually compare on the same figure the Static Pushover (SPO) curve (also known as the Nonlinear Static Procedure curve, FEMA [18]) versus the median (50%-fractile) IDA. Since the SPO curve usually comes in base shear versus θ_{roof} (peak roof drift ratio) coordinates, it needs to be transformed into the IDA's *IM* and *DM* axes. In our case, the θ_{max} response can be easily extracted from the SPO analysis results, while the base shear can be converted to acceleration units by dividing it by the building mass times some (ad hoc) factor (which is close to unity) chosen to make the curves match in their elastic range. By thus plotting the two curves together, as pictured in Figure 9, we see that they correspond to each other. The elastic region of the IDA matches the SPO by construction and the post-yield non-negative SPO segment corresponds to a continuation of the elastic region in the IDA; this is where the IDA is following the familiar "equal displacement" rule for moderate period structures (Veletsos and Newmark [15]). When the SPO turns into a negative slope, the IDA softens and acquires a local slope less than the initial elastic, that gradually decreases till the IDA becomes flat. Essentially, the ending of the SPO at zero strength signals the end of the IDA by the flatline.

This kind of comparison helps us understand clearly what is the meaning of each segment of the SPO curve in terms of the real dynamic response, as represented by the IDA. Perhaps the most striking feature is the apparent disregard of the IDA for the flattening of the SPO. Despite the SPO's reaching of some maximum base shear, the median IDA of this moderate-period structure simply continues on the equal displacement line, as if nothing had happened. Only when the SPO turns negative does the IDA show signs of imminent collapse, which does not come before the SPO actually degrades all the way to zero base shear. Observing these facts, one could stipulate that some more direct, perhaps quantitative rules may be devised to connect the two curves. Actually, one such attempt has been tried out both for single (Vamvatsikos and Cornell [19]) and multi-degree-of-freedom systems (Vamvatsikos and Cornell [20]) with encouraging results.

5   CONCLUSIONS

The step-by-step practical application of Incremental Dynamic Analysis has been demonstrated for a 7-story older reinforced-concrete moment-resisting frame. By using publicly available software it has become almost trivial to perform the analysis, interpolate the IDA curves, estimate limit-state capacities and summarize the results into a format that can be easily integrated with modern PBEE frameworks. IDA offers a complete methodology to handle the abundant data from numerous analyses and calculate the mean annual frequencies of exceeding the specified limit-states. Still, this is only a part of what IDA can provide to the engineering community. It offers valuable intuition when used to investigate the seismic behavior of structures. It can reveal interesting aspects of structural behavior, like the large record-to-record variability, the hardening and softening, the flatline, the structural resurrection and the connection between the IDA and the Static Pushover. This is perhaps the single most important thing to remember: There is a wealth of information that can be found in IDA if only we take advantage of ever-cheaper computing power and automated methods to investigate the structure's behavior.

ACKNOWLEDGEMENTS

REFERENCES

[1]   FEMA. Recommended seismic design criteria for new steel moment-frame buildings. *Report No. FEMA-350*, SAC Joint Venture, Federal Emergency Management Agency, Washington DC, 2000.

[2]   FEMA. Recommended seismic evaluation and upgrade criteria for existing welded steel moment-frame buildings. *Report No. FEMA-351*, SAC Joint Venture, Federal Emergency Management Agency, Washington DC, 2000.

[3]   Vamvatsikos D, Cornell CA. Incremental dynamic analysis. *Earthquake Engineering and Structural Dynamics* 2002; **31**(3):491–514.

[4]   Jalayer F. Direct probabilistic seismic analysis: Implementing non-linear dynamic assessments. PhD Dissertation, Department of Civil and Environmental Engineering, Stanford University, Stanford, CA, 2003. URL http://pitch.stanford.edu/rmsweb/Thesis/.

[5]   PEER. Pacific Earthquake Engineering Research Center - Van Nuys Holiday Inn testbed web-site, 2003. URL `http://www.peertestbeds.net/van%20nuys.htm`. (accessed January 5th, 2003).

[6]   Pincheira JA, Dotiwala FS, D'Souza JT. Seismic analysis of older reinforced concrete columns. *Earthquake Spectra* 1999; **15**(2):245–272.

[7]   Dotiwala FS, D'Souza JT, Pincheira JA. DRAIN2D-UW user's manual. *Report*, Department of Civil and Environmental Engineering, University of Wisconsin, Madison, 1998.

[8]   Powell GH. DRAIN-2D user's guide. *Report No. UCB/EERC-73/22*, Earthquake Engineering Research Center, University of California, Berkeley, CA, 1973.

[9]   Shome N, Cornell CA. Probabilistic seismic demand analysis of nonlinear structures. *Report No. RMS-35*, RMS Program, Stanford University, Stanford, 1999. URL `http://pitch.stanford.edu/rmsweb/Thesis/NileshShome.pdf`. (accessed: June 18th, 2002).

[10]   Vamvatsikos D, Cornell CA. Applied incremental dynamic analysis. *Earthquake Spectra* 2003; In review.

[11]   Vamvatsikos D, Cornell CA. Tracing and post-processing of IDA curves: Theory and software implementation. *Report No. RMS-44*, RMS Program, Stanford University, Stanford, 2002.

[12]   Luco N, Cornell CA. Structure-specific, scalar intensity measures for near-source and ordinary earthquake ground motions. *Earthquake Spectra* 2002; In review.

[13]   Farin G. *Curves and Surfaces for Computer Aided Geometric Design: A Practical Guide*. 2nd edn. Academic Press: San Diego, CA, 1990.

[14]   Lee E. Choosing nodes in parametric curve interpolation. *Computer Aided Design* 1989; **21**(6):363–370.

[15]   Veletsos AS, Newmark NM. Effect of inelastic behavior on the response of simple systems to earthquake motions. In *Proceedings of the 2nd World Conference on Earthquake Engineering*. Tokyo, Japan, 1960; 895–912.

[16]   Cornell CA, Krawinkler H. Progress and challenges in seismic performance assessment. *PEER Center News* 2000; **3**(2). URL `http://peer.berkeley.edu/news/2000spring/index.html`. (accessed: June 18th, 2002).

[17]   Cornell CA, Jalayer F, Hamburger RO, Foutch DA. The probabilistic basis for the 2000 SAC/FEMA steel moment frame guidelines. *ASCE Journal of Structural Engineering* 2002; **128**(4):526–533.

[18]   FEMA. NEHRP guidelines for the seismic rehabilitation of buildings. *Report No. FEMA-273*, Federal Emergency Management Agency, Washington DC, 1997.

[19]   Vamvatsikos D, Cornell CA. Direct estimation of the seismic demand and capacity of oscillators with multi-linear static pushovers through incremental dynamic analysis. *Earthquake Engineering and Structural Dynamics* 2003; In review.

[20]   Vamvatsikos D, Cornell CA. Direct estimation of the seismic demand and capacity of MDOF systems through incremental dynamic analysis of an SDOF approximation. *ASCE Journal of Structural Engineering* 2003; In review.